Inverse analysis of critical current density in a bulk high-temperature superconducting undulator

Ryota Kinjo*
RIKEN SPring-8 Center, 1-1-1, Koto, Sayo-cho, Sayo-gun, Hyogo, Japan

Marco Calvi, Kai Zhang, Sebastian Hellmann, Xiaoyang Liang, and Thomas Schmidt
Paul Scherrer Institut, Forschungsstrasse 111, 5232 Villigen PSI, Switzerland

Mark D. Ainslie, Anthony R. Dennis, and John H. Durrell
Department of Engineering, University of Cambridge, Trumpington Street, Cambridge CB2 1PZ, United Kingdom

(Received 9 September 2021; accepted 31 January 2022; published 8 April 2022)

In order to optimize the design of undulators using high-temperature superconductor (HTS) bulks we have developed a method to estimate the critical current density (J_c) of each bulk from the overall measured magnetic field of an undulator. The vertical magnetic field was measured along the electron-beam axis in a HTS bulk-based undulator consisting of twenty Gd-Ba-Cu-O (GdBCO) bulks inserted in a 12-T solenoid. The J_c values of the bulks were estimated by an inverse analysis approach in which the magnetic field was calculated by the forward simulation of the shielding currents in each HTS bulk with a given J_c. Subsequently the J_c values were iteratively updated using the precalculated response matrix of the undulator magnetic field to J_c. We demonstrate that it is possible to determine the J_c of each HTS bulk with sufficient accuracy for practical application within around 10 iterations. The precalculated response matrix, created in advance, enables the inverse analysis to be performed within a practically short time, on the order of several hours. The measurement error, which destroys the uniqueness of the solution, was investigated and the points to be noted for future magnetic field measurements were clarified. The results show that this inverse-analysis method allows the estimation of the J_c of each bulk comprising an HTS bulk undulator.

DOI: 10.1103/PhysRevAccelBeams.25.043502

I. INTRODUCTION

A short-period, high-field undulator using high-temperature superconductor (HTS) bulks is a promising route for extending the energy of undulator radiation into the high-energy photon region and thus enhancing the photon flux of hard x-ray light in medium-energy storage rings.

HTS-based undulators have several advantages over conventional undulators employing either permanent magnets or low-temperature superconductors. HTS bulks can provide fields an order of magnitude stronger than those generated by permanent magnets; Tomita *et al.* reported a trapped field of over 17 T in a 26-mm diameter Y-Ba-Cu-O (YBCO) bulk at 29 K [1] and Durrell *et al.* reported 17.6 T in a 25-mm diameter Gd-Ba-Cu-O (GdBCO) bulk at 26 K [2]. HTS materials have reduced cooling requirements and are thus more suitable than low-temperature superconductors in high current accelerators, in which the thermal input from the electron beam and the radiation itself is high.

Various approaches to realize a practical HTS undulator have been previously investigated. An undulator using HTS bulks was first proposed in 2004 by Tanaka *et al.* [3]. Tanaka and colleagues subsequently proposed another type of HTS bulk undulator and demonstrated the concept using YBCO bulks [4,5]. In 2007, Tanabe *et al.* demonstrated an undulator using YBCO tape and another using etched MgB_2 film [6]. In 2009, Prestemon *et al.* investigated an undulator using etched YBCO tape [7], Prikhna proposed the application of bulk MgB_2 to undulators [8], and Majoros *et al.* investigated an undulator using MgB_2 multifilamentary wire [9]. In 2017, Kesgin *et al.* proposed a winding scheme for an HTS tape undulator and demonstrated the generation of the undulator field [10].

HTS tape-based undulators have the advantage, compared to bulks, of being more suitable for series production, they have more homogeneous properties and the undulator field can be easily controlled with an external power

*ryota.kinjo@psi.ch
Present address: Institute of Advanced Energy, Kyoto University, Gokasho, Uji, Kyoto, 611-0011, Japan.

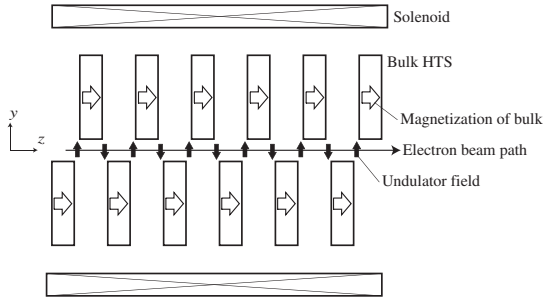

FIG. 1. Principle of the HTS-bulk staggered-array undulator, HSAU (side view). The solenoid coil induces the magnetization of the HTS bulks which then generate the y-direction field.

supply. On the other hand, the engineering critical current density (J_e) is lower than that for bulks because of the presence of both substrate (Hastelloy or stainless steel) and stabilizer (typically copper or silver) layers.

While the higher J_e of HTS bulks makes them ideal for strong-field undulators, the HTS bulk-based undulators need to be magnetized using a complex structure such as Refs. [3–5]. A practical HTS undulator would ideally be simpler in conception.

The undulator under investigation here is the HTS-bulk staggered-array undulator (HSAU) [11–13]. A schematic diagram of the HSAU is shown in Fig. 1. When a solenoid field is applied to the HTS bulks in the z-direction, superconducting current loops with a current density equal to the critical current density as predicted by Bean's critical state model [14] are established to minimize the change in the magnetic field inside the HTS bulks. They are thus magnetized in the z-direction and provide a sinusoidal magnetic field in the y-direction along the electron-beam path. In this type of undulator, the HTS bulks can be magnetized simultaneously using one solenoid because the magnetization direction is the same for all of them. The undulator field strength can also be tuned by varying the solenoid field. This avoids the expensive and heavy mechanical frame essential to a permanent magnet undulator, where the field can be tuned only by varying the distance between the magnetic rows. Considering the large forces in a high-field undulator and the fact that cracking in the HTS bulks occurred in the demonstration experiment of Ref. [5], a nonmovable structure is a distinct advantage. So far, an undulator field of $B_0 > 0.8$ T was achieved at 6 K and 20 K in a 6-period, 10-mm-period, 4-mm-gap prototype with a 2 T superconducting solenoid and a helium gas cooling system [15,16].

Currently, the Paul Scherrrer Institute (PSI) is conducting research toward the practical application of the HSAU as a bright source for the new microscopy tomography (I-TOMCAT) beamline of the upgrade of the Swiss Light Source, SLS 2.0. In the preliminary experiments conducted so far, the amplitude of the undulator magnetic field was as expected. However, the variation of the field amplitude among poles is not compatible yet with the high spectral purity required for an undulator, especially if operated with higher harmonics. While the variation in the magnetic field strength in permanent magnets typically used for undulators is about 1% or less, those in HTS bulks are much more. This is a consequence of the growth process for bulks; however, it would be expected that mass production would bring closer control of production and reduce sample-to-sample variability. Furthermore, the individual differences in J_c become more noticeable in the high magnetic field region [15]. For these reasons, refining the magnetic field of the HTS bulk undulator is currently the most challenging issue. Fortunately, in the I-TOMCAT beamline, we plan to fix the magnetic field strength of the HSAU to a certain value and change the wavelength by selecting a different harmonic. Therefore, the first goal of the field tuning is to obtain strong uniformity of the magnetic field only under specific operating conditions.

The adjustment strategies for the magnetic field in conventional undulators using permanent magnets can be broadly divided into two types depending on the measurement method. The first strategy is to measure the characteristics of all magnets individually in advance and determine the ideal arrangement of the magnets. The second strategy is to measure the magnetic field distribution of the undulator after arranging the magnets on a rigid metal support and make *in-situ* adjustments. For the latter strategy, adjustments can be made by swapping the magnet position (sorting), by fine-tuning the distance of the magnet from the electron beam axis, by applying small movable (rotatable) magnets as booster magnets, or by placing thin ferromagnetic plates on the surface of the magnet. In any of the above mentioned cases, it is necessary to identify the magnetic signature of each magnet to distinguish its contribution from the overall magnetic field profile of the undulator.

The same strategies can be considered for the HTS bulk undulator. The former strategy has the advantage of using an accurately measured characteristic of each HTS bulk, but has the disadvantage that it takes a considerable amount of time to cool, measure, and raise the temperature of hundreds of bulks. In addition, there is a drawback that errors in the assembled undulator, including nonuniformity of the solenoid magnetic field and deformation occurring during cool-down cannot be considered. The latter strategy does not have those drawbacks, but requires the extraction of the magnetic field components created by a particular HTS bulk from the overall undulator magnetic field distribution. In other words, it is necessary to estimate the current distribution in each HTS bulk from the measured undulator magnetic field and use that information to adjust the magnetic field.

Inverse analysis of the current distribution from the measured magnetic field is a difficult challenge as it deals with superconductivity-related electromagnetic problems which essentially involve the inversion of the Biot-Savart law. To date, inverse analyses have been made using a

variety of inversion methods. The so-called matrix method that solves multiple algebraic equations has commonly been used [17–22], as well as the fast Fourier transform [23]. Takeda *et al.* used the generic algorithm and reported greater robustness than the matrix methods if there is a large amount of noise (10%) in the measurement data [24]. These are particularly effective for estimating the current distribution inside HTS thin films or bulks where the J_c is inhomogeneous or local current loops exist due to grain boundaries and growth conditions. On the other hand, in the HSAU, since the measurable region is limited to a small volume near the z-axis, sufficient magnetic field data cannot be obtained to perform an inversion of the Biot-Savart law. Therefore, this paper focuses the target of the inverse analysis on the most dominant parameter to the uniformity of the undulator field, i.e., the critical current density J_c of each bulk. We assume that each bulk is a perfect, high-quality single-domain superconductor and any current-density inhomogeneity in J_c is negligible. Thus the current distributions are obtained by a forward shielding-current simulation using J_c as the input. This method has the advantage that the relationship between the current distribution and the magnetic field distribution is always consistent.

In this paper, we propose a method to inversely analyze the J_c of each bulk from the measured on-axis magnetic field as a first step of the field tuning. Our method combines a forward HTS simulation using the H-formulation in COMSOL Multiphysics with the implemented matrix method.

II. METHOD

A. Experimental setup

Experiments were performed in a 12-T solenoid at the University of Cambridge equipped with a large bore variable temperature insert. The samples used were $GdBa_2Cu_3O_{7-\delta}$ bulk materials prepared by the top seeded melt growth technique [25] at the University of Cambridge, cut into semicircles of diameter 30 mm and with a thickness of 4 mm. The samples are then placed in copper holders of diameter 40 mm and thickness 5 mm with a sample space 4 mm deep, filled with epoxy and fixed. A stack of 20 of these holders is placed in a cryostat and cooled to a cryogenic temperature with helium gas and a heater. The Hall probe is calibrated to cryogenic temperatures at PSI, and the thermal voltages are canceled by switching positive and negative currents. A photograph of the experimental setup is shown in Fig. 2 and details of the experiment are described elsewhere in the paper for the previous experimental campaign [26].

B. Matrix method for inverse analysis of J_c

In order to calculate the undulator magnetic field based on the given J_c data, we used the E–J power law for a type-II superconductor [27]:

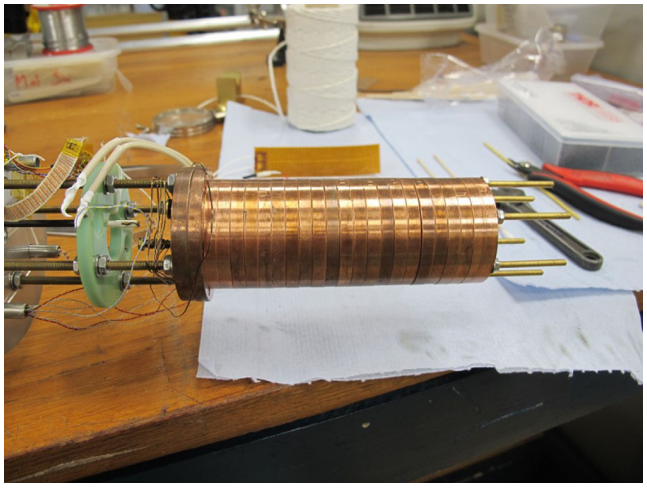

FIG. 2. Experimental setup. The 5-mm-thick copper holders, in which the 4-mm-thick HTS bulks are placed, are stacked on the end of the measurement system with a temperature sensor. This is installed into the cryostat with the 12-T solenoid.

$$\mathbf{E} = E_c \frac{\mathbf{J}}{|\mathbf{J}|}\left(\frac{|\mathbf{J}|}{J_c}\right)^n \tag{1}$$

The parameters and variables used in the simulation are given in Table I. The simulations are carried out using the commercial finite-element software, COMSOL Multiphysics 5.5 [28], which implements the finite element method to solve Maxwell's equations using the H-formulation [29–32].

Figure 3 shows the two-dimensional geometry for the simulations. Twenty bulks are lined up in a large air domain, as in the experiment. The z-direction solenoidal field is applied to the horizontal boundaries and a "perfect magnetic field" constraint (such that $\mathbf{n} \times \mathbf{H} = 0$) is applied to the vertical boundaries. The copper parts supporting the HTS bulks in the experiments are treated as air in the simulation. The solenoid field is changed from $B_{s,\mathrm{start}}(=8\ \mathrm{T})$ at $t = 0$ s to B_s $(=7$ to $0\ \mathrm{T})$ at $t = 10500$ s, and maintained until $t = 20000$ s. Field-cooling magnetization was simulated using the time-dependent H-formulation model with an initial condition of $B_s = 8$ T, which is then ramped down to a particular value via a function applied as

TABLE I. Parameters and variables used in the simulation.

Period length	λ_u [mm]	10
Gap	g [mm]	4
Number of periods	N_u	10
Number of bulks	N	20
Bulk height	D_y [mm]	15
Bulk thickness	D_z [mm]	4
Index for E-J power law	n	20 (Ref. [31])
Critical field	E_c [V/m]	10^{-4}
Number of observation points	M	
Normalized J_c of ith bulk	p_i	

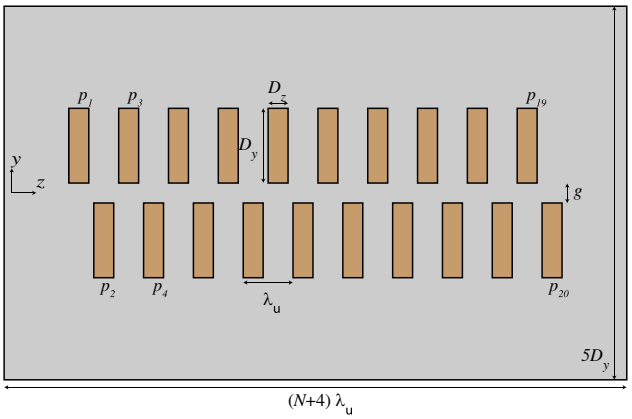

FIG. 3. Simulation geometry for the inverse analysis. Twenty bulks having different parameters, p_i, are aligned in a large air domain. The z-direction solenoid field is applied to the top and bottom boundaries and a perfect magnetic field constraint (such that $\mathbf{n} \times \mathbf{H} = 0$) is applied to the left and right boundaries.

the boundary conditions, then held at that value, as described in Ref. [33].

The variable p_i represents J_c of the ith bulk ($1 \le i \le 20$) normalized by 10 kA/mm^2 (expected J_c at 10 K and zero field), and is estimated in the inverse analysis.

Let us consider an inverse analysis of J_c inside N HTS bulks from the measured magnetic field data at M observation points along the z-axis $\mathbf{z}$. The normalized J_c values of the bulks are represented by the N-element vector $\mathbf{p}$, the measured B_y is represented by the M-element vector $\mathbf{B}_{\mathrm{exp}}$, and the calculated B_y is represented by the M-element vector $\mathbf{B}_{\mathrm{sim}}$. Here, $\mathbf{B}_{\mathrm{exp}}$ is a function of p, but it is nonlinear and cannot be solved directly. The response of $\mathbf{B}_{\mathrm{sim}}$ when $\mathbf{p}$ is changed, is represented by the $M \times N$ matrix $\mathbf{A}$:

$$\mathbf{A} = \frac{1}{\alpha} \times [\,\Delta\mathbf{B}_{\mathrm{sim},1} \quad \Delta\mathbf{B}_{\mathrm{sim},2} \quad \cdots \quad \Delta\mathbf{B}_{\mathrm{sim},N}\,], \tag{2}$$

$$\Delta\mathbf{B}_{\mathrm{sim},i} = \mathbf{B}_{\mathrm{sim},i} - \mathbf{B}_{\mathrm{sim},0}. \tag{3}$$

Here, $\mathbf{B}_{\mathrm{sim},0}$ is the simulation result using the parameter set $\mathbf{p}_0$ in which all terms are equal to p and $\mathbf{B}_{\mathrm{sim},i}$ is the simulation result using the parameter set $\mathbf{p}_i$ in which the ith term p_i rises from p to $p + \alpha$.

$$\mathbf{p}_0 = (p, \ldots, p, \ldots, p), \tag{4}$$

$$\mathbf{p}_i = (p, \ldots, p + \alpha, \ldots, p). \tag{5}$$

The response matrix $\mathbf{A}$ is similar to the Jacobian. By using this matrix, $\mathbf{p}$ can be updated iteratively. In the kth iteration, $\mathbf{p}^{k+1}$ is derived from $\mathbf{p}^k$ by solving the linear equation

$$\mathbf{A}\Delta\mathbf{p}^k = (\mathbf{B}_{\mathrm{exp}} - \mathbf{B}^k_{\mathrm{sim}}) \tag{6}$$

and then by,

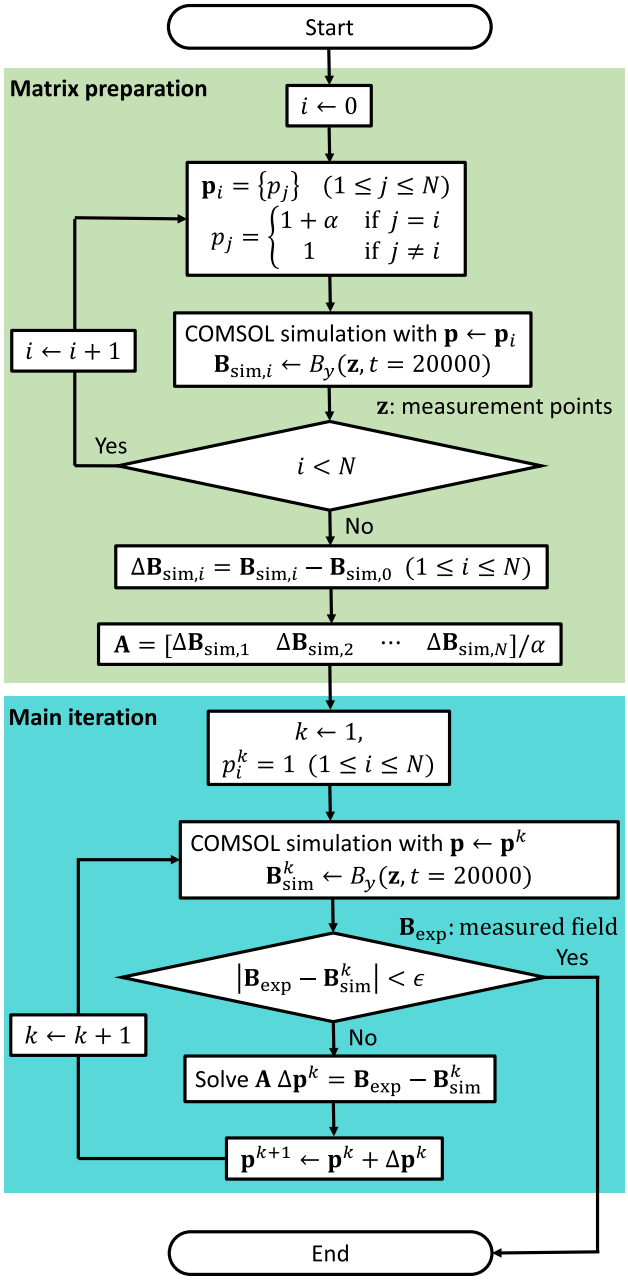

FIG. 4. Flowchart of the inverse analysis.

$$\mathbf{p}^{k+1} = \mathbf{p}^k + \beta\Delta\mathbf{p}^k \tag{7}$$

In the above equations, α and β are the response and damping factors and their empirically reasonable values are 0.25–0.5 and 0.1–0.2, respectively. This algorithm of the matrix method was implemented using Java in the application builder of COMSOL Multiphysics and Eq. (6) was solved by the decomposition functions in the Apache Commons Math library [34]. Figure 4 shows the flowchart of the inverse analysis.

Unlike other common nonlinear inverse problems, $\mathbf{A}$ is not updated during each iteration in order to reduce the

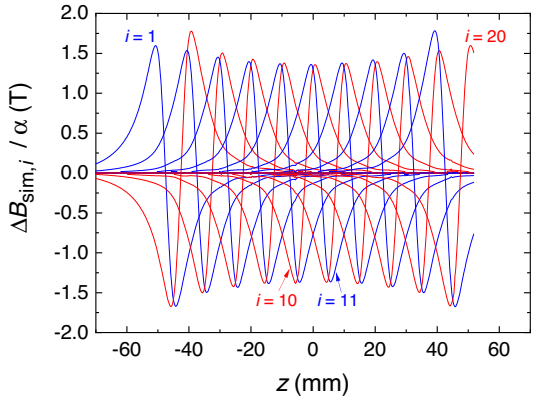

FIG. 5. Response of B_y to J_c change. This example is calculated from the change in B_y when each lift factor p is changed from 0.5 to 0.75 ($\alpha = 0.25$) for $B_{s,\mathrm{start}} = 8$ T and $B_{s,\mathrm{end}} = 3$ T. The blue lines are for the upper (odd i) bulks and the red lines are for the lower (even i) bulks.

calculation time. An example of $\Delta\mathbf{B}_{\mathrm{sim},i}/\alpha(1 \le i \le N)$ with $B_{s,\mathrm{start}} = 8$ T, $B_{s,\mathrm{end}} = 3$ T, $p = 0.5$ and $\alpha = 0.25$ is shown in Fig. 5. Here, all the responses were calculated by updating the J_c of each HTS bulk. However, one can also create the matrix by translating the response of a certain i to all other columns. In such a case, the initial time cost required to create the matrix is $1/N$ times the original.

C. Validation check

To verify the validity of the matrix method, the inverse analysis was performed with the given $\mathbf{p}$ by the random generator. First, the forward simulation was performed with given $\mathbf{p}$ ($N = 6$) that follow a normal distribution with a mean of around 1.0 and a standard deviation σ_p of between 0.05 and 0.4. Then, the unknown $\mathbf{p}$ was calculated by the inverse analysis using the matrix method and compared with the given $\mathbf{p}$. Figures 6(a) and 6(b) show the root mean square (RMS) error between the given $\mathbf{p}$ and estimated $\mathbf{p}$, and the RMS error between the input and the output magnetic fields, at each σ_p, respectively. As shown in the graph, the matrix method can estimate $\mathbf{p}$ with sufficient accuracy ($<0.1\sigma_p$) within about 10 iterations. Next, we compared the matrix method with the general-purpose algorithms implemented in the optimization module of COMSOL Multiphysics. Figure 6(c) compares the relations between the RMS error of the magnetic field and the number of iterations from using different numerical methods but with the same input data. Here, "coordinate search" is an algorithm that changes the control variables one by one [35], and bound optimization by quadratic approximation (BOBYQA) is one of the trust-region algorithms and assumes a quadratic objective function [36]. It should be mentioned that before starting optimization, the BOBYQA method needs $2N + 1$ iterations to find the quadratic function and the matrix method needs N

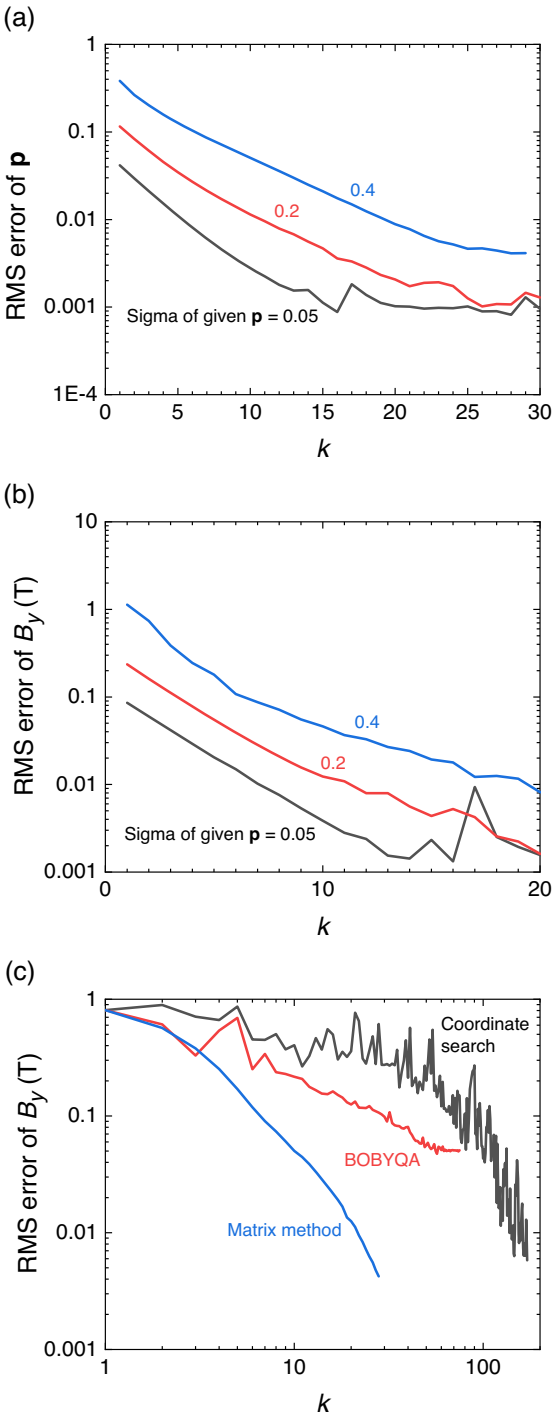

FIG. 6. RMS difference of (a) given and estimated $\mathbf{p}$ and (b) input and output B_y, for $\sigma_p = 0.05$, 0.2 and 0.4. (c) Comparison of the conversion of the matrix method with the general-purpose optimization algorithms.

iterations to find the response matrix. These preiteration steps are omitted in the comparison plot. It can be concluded that the matrix method converges more quickly and is more stable compared to the general-purpose optimization algorithms. Because one forward simulation

needs almost 30 minutes for the 2-D bulk HTS undulator model ($N = 20$) with a normal workstation (Intel Xeon E3-1241 v3 3.5 GHz 8 logical cores and 16 GB memory), quick convergence greatly reduces the total calculation time.

One caveat here is that we did not use the gradient-based general-purpose algorithms implemented in COMSOL, which may be faster for some kind of problems than "coordinate search" or BOBYQA. This is because the gradient-based algorithms did not converge for this particular problem. One possible reason is the high nonlinearity of $\mathbf{E}$ to the control variable, as in Eq. (1). However, even with an alternative control variable $p_i' = p_i^n \ (1 \le i \le N)$ which linearizes the equation, the calculation still did not converge.

III. RESULTS AND DISCUSSION

A. Experiment results

The results obtained during the most recent experimental campaign at the University of Cambridge are shown in Fig. 7 which plots the change in the B_y profile during field-cooling magnetization (the solenoid field B_s decreases linearly from 8 T) at (a) 10 K and (b) 20 K. A B_y offset proportional to the strength of B_s is subtracted before any data analysis to compensate the angular error of the probe, estimated to be ~5°.

We defined the undulator field B_0 by the average amplitude of B_y in the central 15 peaks. In Figs. 7(c) and 7(d), B_0 and its relative standard deviation are plotted, respectively. It can be seen that B_0 has dropped at $B_s = 1$ T ($\Delta B_s = 7$ T) at 10 K. At the same time, a temperature rise was observed before reaching $\Delta B_s = 7$ T, indicating a quench occurred. Also in a previous experiment, a quench occurred at around $\Delta B_s = 6$–7 T. On the other hand, this does not occur at 20 K, where the sweep speed of B_s is slower than 10 K. This appears to be because of the temperature rise due to the movement of the magnetic flux inside the HTS bulks when ΔB_s rises. To confirm this, an experiment at 10 K and at a slow ramp rate is planned. To avoid this quench, we are planning to use shrink-fit copper plates in the future setup, in which the HTS bulks will be compressed well to minimize the tensile stress induced by large magnetic forces at large ΔB_s. In the meantime, better

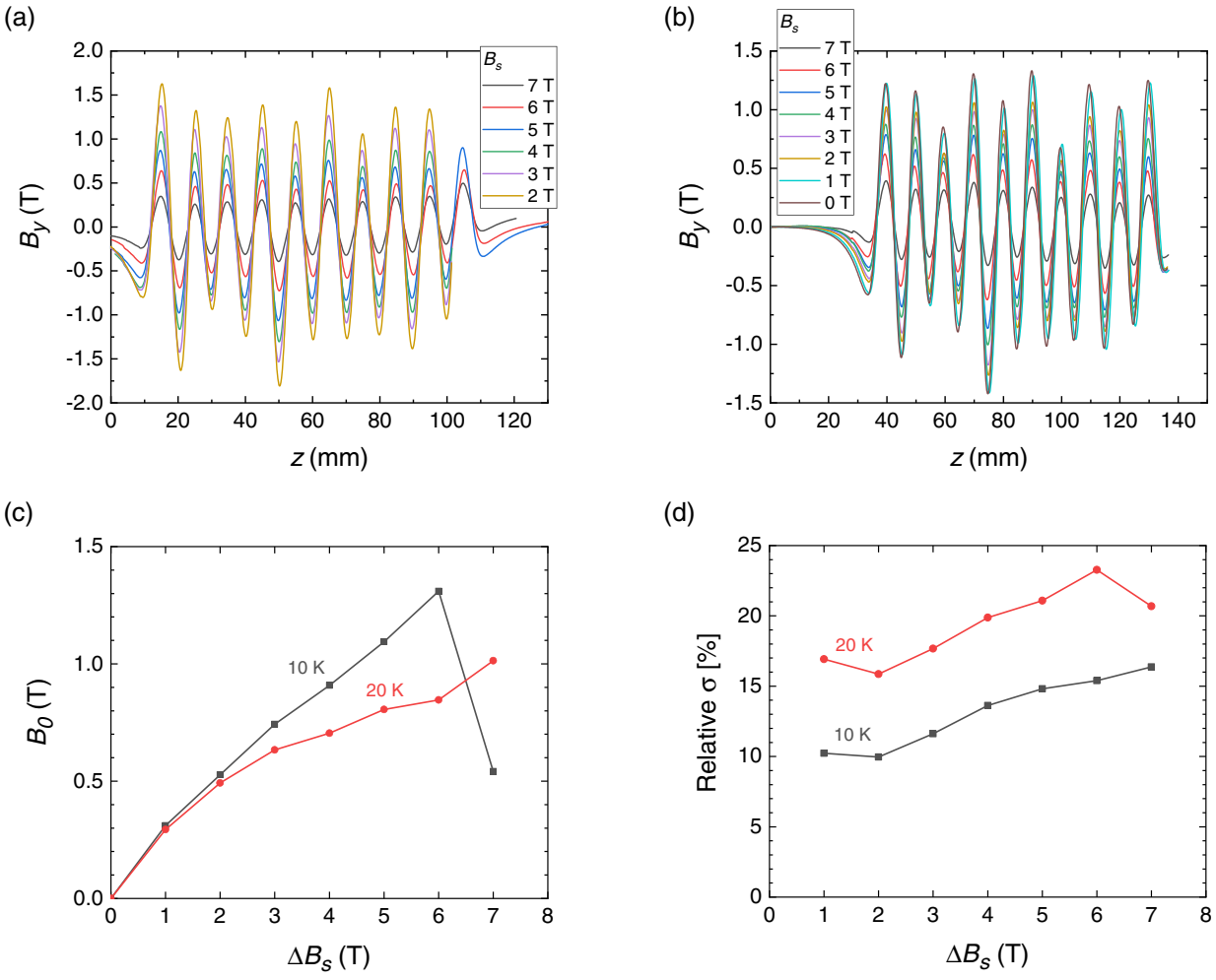

FIG. 7. Measured magnetic field B_y when the solenoid field is changed to B_s after field cooling with 8 T for operating temperatures of (a) 10 K and (b) 20 K; the relationship between (c) ΔB_s and B_0, and (d) ΔB_s and the relative standard deviation of B_0.

thermal connection to the sample holder and the cooling system can be obtained.

Figure 7(c) shows that the B_0 values for 10 K and 20 K are of a similar magnitude for small ΔB_s, but B_0 for 10 K is higher than that for 20 K for large ΔB_s. This is because the cross-sectional area over which the magnetizing current flows is smaller for a higher current density (at 10 K) and larger for a lower current density (at 20 K). In the latter

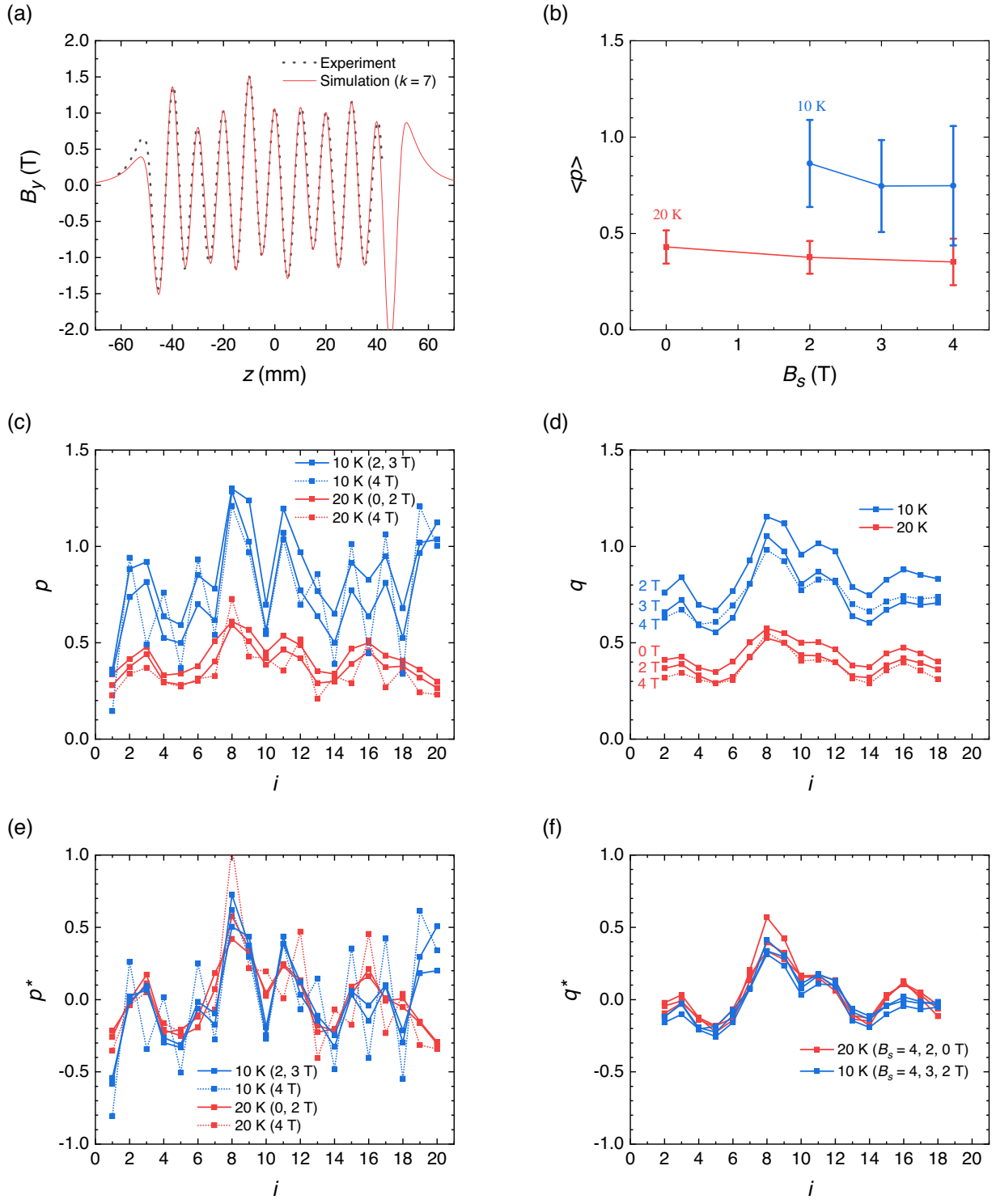

FIG. 8. Results of inverse analysis; (a) the comparison of measured and simulated B_y, (b) the average and the standard deviation of the estimated $\mathbf{p}$ for each T and B_s; each value of estimated (c) $\mathbf{p}$ and (e) $\mathbf{p}^*$ and (d, f) the local weighted average of these to cancel the zigzag error.

case, the current flows in regions far from the z-axis. The relative σ value is larger at 20 K than at 10 K for a similar reason; the relative σ value is also affected by the position error of the bulks, especially in the y-direction, and by the measurement error of B_y. However, the dominant factor is individual differences in J_c of the HTS bulks (see the Appendix A for a discussion on the measurement error).

At any rate, the subject of this paper is the estimation of J_c from the measured magnetic fields for future field tuning to reduce the relative σ value to a practical level as a light source.

B. Inverse analysis results

The inverse analysis of J_c was performed using the matrix method so as to reproduce the magnetic field distribution of the experiment presented in the previous section. Figure 8(a) shows an example of magnetic field profile as a result of the experiment and the inverse analysis. The results match well except for the edges, i.e., the end bulks. Because the shape of the end magnetic field differs between 2D and 3D calculations, and the end magnetic field is greatly affected by measurement errors as described in Appendix A, it is therefore meaningless to require a strict overlap between the simulated and the experimental B_y at both ends of our present 2D HTS undulator model. Figure 8(b) shows the average of the estimated $\mathbf{p}$, $\langle p \rangle = \sum p_i/N$, and its standard deviation for each T and each B_s as the result of the inverse analysis. This indicates the general superconducting property that J_c is larger when T and B are smaller, and also indicates the greater variation in J_c between individual bulks. Figure 8(c) shows the estimated p_i for each T and B_s. It can be seen that there are individual differences of up to about 50% in the critical current densities of the 20 HTS bulks used in this experiment. For example, bulk #8 has a J_c nearly double that of #5.

Figure 8(e) shows $\mathbf{p}^*$. Here, $\mathbf{p}^*$ is the deviation from the average defined by

$$p_i^* = \frac{p_i - \langle p \rangle}{\langle p \rangle}. \tag{8}$$

For low B_s (solid curve), the results are consistent, while at $B_s = 4$ T (dotted curve), the results are significantly different. Of course there are individual differences not only in J_c at a certain T and a certain B, but also in the $J_c(B,T)$ curve; however, the cause of these discrepancies is the nonuniqueness of the solution caused by the measurement error. From the shape of the dotted lines, we call this "zigzag error," and this will be discussed in detail in Sec. C.

To evaluate the results canceling the zigzag error, we introduce the local weighted average $\mathbf{q}$ given by

$$q_i = \frac{p_i}{2} + \frac{(p_{i-1} + p_{i+1})}{4} \qquad (2 \le i \le M-1). \tag{9}$$

Figures 8(d) and 8(f) show the local average of $\mathbf{q}$ and its deviation from average $\mathbf{q}^*$, respectively. It shows that the J_c differences between all HTS bulks are consistent even under different T and B conditions. It should be noted that $\mathbf{q}$ and $\mathbf{p}$ do not mean the same thing, but this result shows that the estimation is working appropriately and the actual $\mathbf{p}$ can also be consistent if there is no measurement error.

Figure 9 shows an example of the current density distribution, after the 10th iteration of the inverse analysis for $T = 10$ K and $B_s = 3$ T. Because this inverse analysis is not a simple inversion of the Biot-Savart law but is a result of applying the forward HTS simulation, the magnetization current flows from the outer side of the bulk and the area of the final current profile for each bulk is consistent with its estimated J_c (vector $\mathbf{p}$) naturally.

C. Systematic error problem in inverse analysis

In the undulator, the magnetic field is generated by the upper and lower magnets. There are, therefore, an infinite number of combinations of upper and lower magnets which can produce the same B_y at a certain point on the

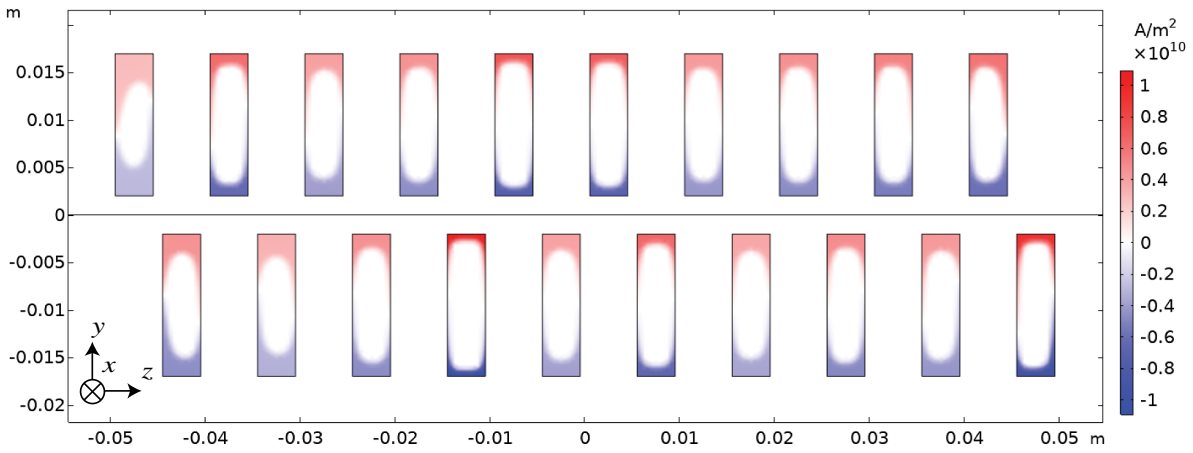

FIG. 9. Current density distribution (J_x) after the 10th iteration of the inverse analysis for $T = 10$ K and $B_s = 3$ T.

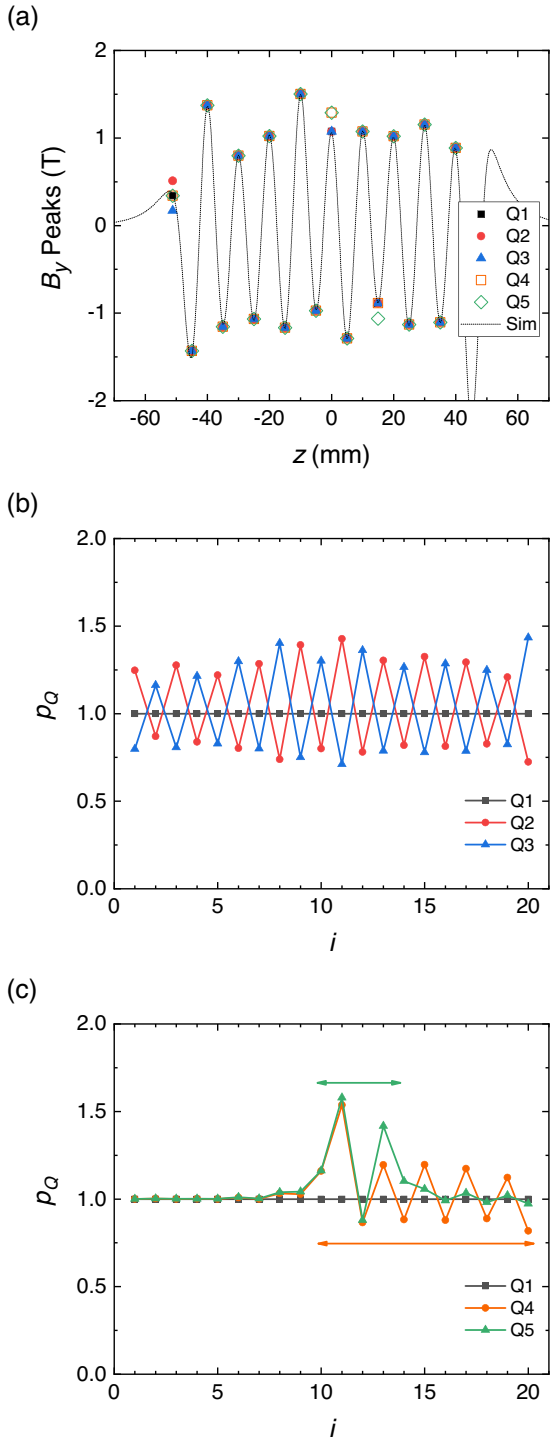

FIG. 10. The zigzag effect of the local offset to the inverse analysis; (a) five input data sets for the inverse analysis, and the estimated **p** for (b) the single positive or negative offset at the left end and (c) the single or double offset in the middle.

electron-beam axis. In the case where the number of observation points M is much larger than the number of HTS bulks N, in such a least squares problem, the random error of the measurement is not a major issue in the inverse analysis. However, this is not the case when systematic errors exist. This section describes the problem of a unique solution of **p** in the inverse analysis for the HSAU. As shown in Appendix A, systematic measurement errors can result in a local magnetic field increase / decrease at the edges. Therefore let us first investigate how the inverse analysis is affected by the change in the magnetic field distribution at both ends. Here, in order to easily create input data, only the peaks of B_y along the electron-beam axis are considered as the observation points, and the inverse analysis is performed under the condition of $M < N$ (but the same phenomenon can be confirmed even in the case of $M \gg N$). As shown in Fig. 10(a), the input data at the left end are set to (Q1) 0.34 T (original), (Q2) $+0.17$ T higher than the original, (Q3) -0.17 T lower than the original, and the right end is set to be free, i.e., no particular value.

The estimated p_Q, normalized to p obtained by data Q1, are plotted in Fig. 10(b). For data Q2, the upper bulks have larger normalized J_c values, and for data Q3, the lower bulks have larger normalized J_c values. The normalized J_c values for both data Q2 and data Q3 show clear zigzag effects. Thus, p_i cannot be uniquely determined by the magnetic field distribution near the bulk, but by the overall magnetic field including the ends. Similarly, Fig. 10(c) shows the zigzag results calculated for two special test cases if we artificially manipulated the local peaks like in Q4 and Q5 in Fig. 10(a). The data Q4 which has a large peak at $z = 0$ mm, and the data Q5 which has large peaks at $z = 0$ and 15 mm. This indicates that a region in which the upper bulks have a large J_c value is created locally. The real zigzag error in Fig. 8(c) and 8(e) is a result of the superposition of these zigzag errors.

In the inverse analysis of the HSAU, accurate magnetic field measurement data without systematic errors is essential. On the other hand, since in HTS undulators it is required that magnetic field measurements are carried out in small apertures and under low temperatures within vacuums, it is challenging to perfect the magnetic field measurement, and it is important to ensure an error-resistant redundancy. For example, adding multiple B_y probes separated in the y-direction like $y = -0.5, 0, +0.5$ mm and a B_z probe would contribute to better analysing the zigzag problem in the inverse analysis.

IV. SUMMARY

In order to permit field tuning of a HTS-bulk staggered-array undulator (HSAU) to ensure high field uniformity it is vital to obtain accurate values of J_c for each of the individual bulks comprising the undulator. We have shown here that an inverse analysis method which combines a forward HTS simulation using the H-formulation implemented in COMSOL Multiphysics and the matrix method can work well for this purpose. Using this approach we were able to determine the J_c of each bulk in the HSAU from its measured magnetic field. The matrix method

generated results with sufficient accuracy for practical application ($<0.1\sigma_p$) within around 10 iterations, even with a fixed response matrix created in advance. This approach reduces the computational cost drastically compared with other general-purpose algorithms. We further determined, in the inverse analysis of the experimental data, that the systematic measurement error even in the local region (local offset of the field) destroyed the uniqueness of the solution throughout all the bulks; we described this effect as "zigzag error." The zigzag error can also be caused by the measurement error of the field peak at the ends or the center, which should be reduced by minimizing the probe tilt and offset, or by simultaneously measuring B_z in future experiments. By omitting the global zigzag error, reasonable J_c values for all HTS bulks could be obtained.

As a future application of the method, it is conceivable to perform an inverse analysis incorporating the off-axis magnetic fields, which may cause undesired effects on the electron beam like lensing due to a magnetic field multipole. The matrix method can also be adopted for field tuning, in which the positions of the bulks or the ferromagnetic poles will be the control variables and the magnetic field peaks or local field integrals will be the objective function.

ACKNOWLEDGMENTS

This work was done under the auspices of CHART (Swiss Accelerator Research and Technology Collaboration, [38]). M D Ainslie would like to acknowledge financial support from an Engineering and Physical Sciences Research Council (EPSRC) Early Career Fellowship, EP/P020313/1. All data are provided in full in the results section of this paper. R. K. would like to acknowledge his present institution, Institute of Advanced Energy, Kyoto University. The authors would like to thank Dr. Marek Bartkowiak from Paul Scherrer Institut for calibrating Hall sensors with PPMS.

APPENDIX A: CAUSE OF MEASUREMENT ERROR

Here, the cause of the error in the measurement of B_y will be clarified. The main causes of the error are probe tilt and offset, and B_z contamination. In Fig. 11 the difference in the magnetic field distributions from the ideal case (a) when the measurement line is tilted by 0.5 degrees and (b) when the probe is offset by 0.5 mm are shown. It can be seen that the magnetic field changes significantly, especially at the ends. When there are magnets on both the top and bottom, the change in magnetic field due to probe offset is small, whereas at the ends of the experimental setup, in which the magnet is on either the top or bottom, a large error occurs. Figure 11(c) shows the B_z component that contaminates

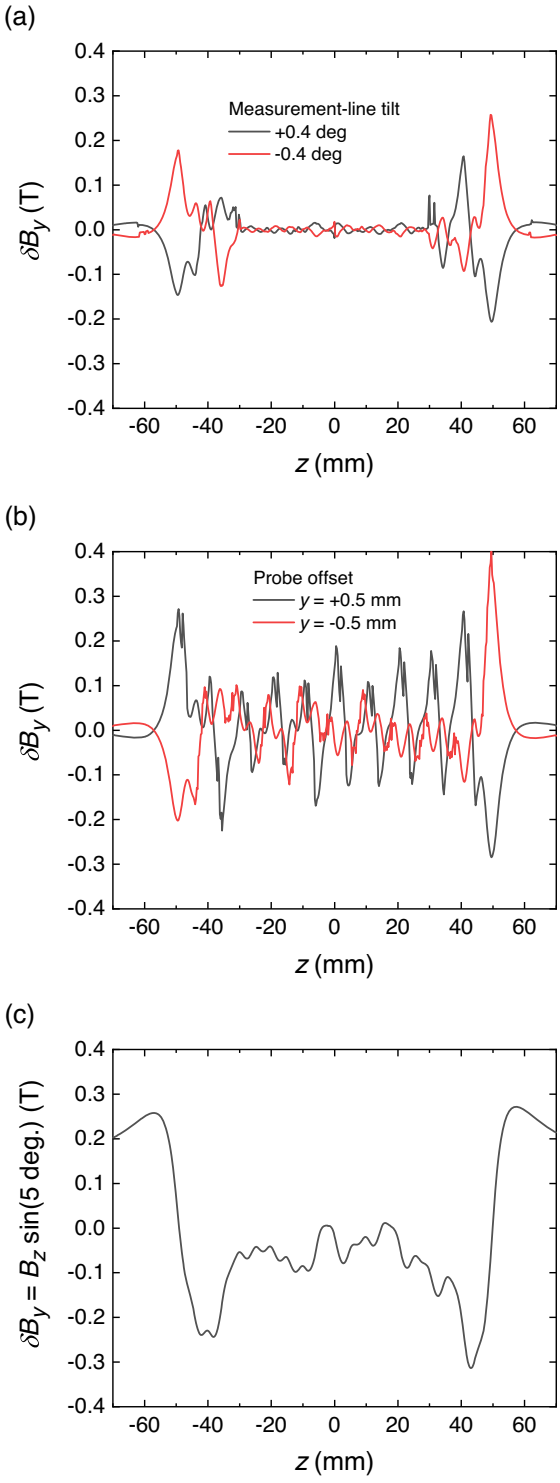

FIG. 11. Error sources for the measurement. Error due to (a) the tilt of the measurement line, (b) the probe offset in the y-direction, and (c) the contamination of B_z due to the probe pitching. The simulation was carried out with $B_s = 3$ T and the estimated $\mathbf{p}$ in Sec. III B.

B_y when the probe is tilted 5 degrees at $B_s = 3$ T, like our experiment. The B_z contamination is not a constant, although we assumed a constant offset for Figs. 7(a)

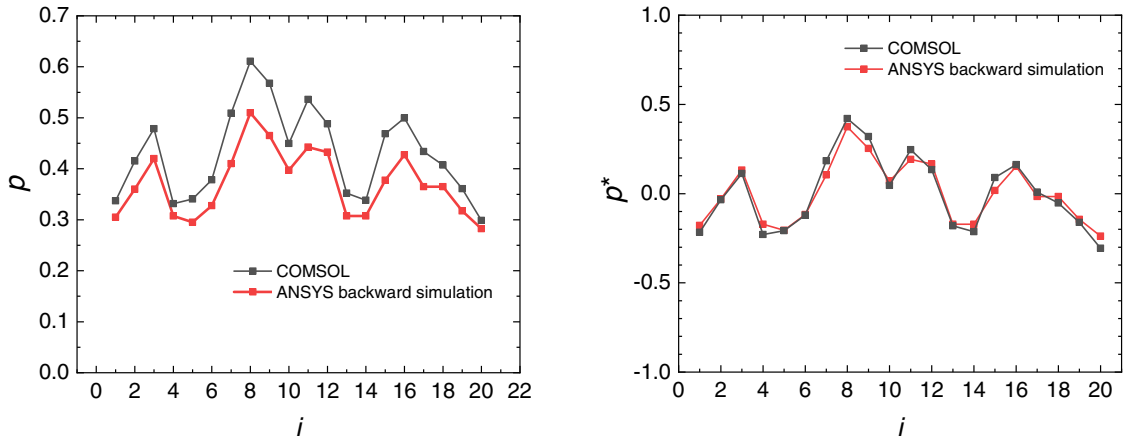

FIG. 12. Comparison of the results of the inverse analysis with the ANSYS backward computation method for 20 K and $B_s = 2$ T.

and 7(b). This also causes an error in the inverse analysis. It is important to design and perform experiments while paying attention to the points clarified here.

APPENDIX B: COMPARISON WITH THE ANSYS BACKWARD COMPUTATION METHOD

The matrix method has also been demonstrated in another finite-element-method software, ANSYS, using the **A**-V formulation based backward computation method [33,37]. The backwards calculation gives a critical state solution in the HSAU; this is similar to the condition when $n = \infty$ in Eq. (1). In the ANSYS simulation, the magnetic field dependent $J_c(B)$ at 10 K, as shown in Eq. (1), is set as the baseline. Each superconducting bulk is considered to have a normalized J_c to this $J_c(B)$ (lift factor).

$$J_c(B) = J_{c1}\exp\left(-\frac{B}{B_L}\right) + J_{c2}\frac{B}{B_{\max}}\exp\left[\frac{1}{y}\left(1-\frac{B}{B_{\max}}\right)^{y}\right] \tag{B1}$$

where J_{c1}, J_{c2}, B_L, $B_{\max}$, and y are 1.0×10^{10} A/m^2, 8.8×10^{9} A/m^2, 0.8 T, 4.2 T, and 0.8, respectively.

Figure 12(a) shows a comparison of the lift factors calculated using the ANSYS backward computation and the **p** calculated using COMSOL and the H-formulation. Figure 12(b) compares the values of $\mathbf{p}^*$ calculated by the two softwares. The difference in the absolute value of **p** comes from the fact that Eq. (B1) and the critical state model is used in the ANSYS backward simulation. However, Fig. 12(b) shows nice agreement for $\mathbf{p}^*$. This means that, from the viewpoint of field tuning, which needs only the relative difference of J_c, the inverse analysis is not sensitive to the simulation method and any uncertain parameter assumptions in the HTS simulation: for example, the real E–J relation or $J_c(B)$ curve of the HTS bulk.

[1] M. Tomita and M. Murakami, High-temperature superconductor bulk magnets that can trap magnetic fields of over 17 Tesla at 29 K, Nature (London) **421**, 517 (2003).
[2] J. H. Durrell, A. R. Dennis, J. Jaroszynski, M. D. Ainslie, K. G. B. Palmer, Y.-H. Shi, A. M. Campbell, J. Hull, M. Strasik, E. E. Hellstrom, and D. A. Cardwell, A trapped field of 17.6 T in melt-processed, bulk Gd-Ba-Cu-O reinforced with shrink-fit steel, Supercond. Sci. Technol. **27**, 082001 (2014).
[3] T. Tanaka, T. Hara, H. Kitamura, R. Tsuru, T. Bizen, X. Maréchal, and T. Seike, Application of high-temperature superconducting permanent magnets to synchrotron radiation sources, Phys. Rev. ST Accel. Beams **7**, 090704 (2004).
[4] T. Tanaka, R. Tsuru, and H. Kitamura, Pure-type superconducting permanent-magnet undulator, J. Synchrotron Radiat. **12**, 442 (2005).
[5] T. Tanaka, T. Hara, R. Tsuru, D. Iwaki, T. Bizen, X. Marechal, T. Seike, and H. Kitamura, Utilization of bulk high-temperature superconductors for shorter-period synchrotron radiation sources, Supercond. Sci. Technol. **19**, S438 (2006).
[6] T. Tanabe, D. A. Harder, G. Rakowsky, T. Shaftan, and J. Skaritka, Insertion device R & D for "NSLS-II", in *Proceedings of PAC07, Albuquerque, New Mexico, USA* (IEEE, New York, 2007).
[7] S. Prestemon, D. Dietderich, A. Madur, S. Marks, and R. Schlueter, High performance short-period undulators using high temperature superconductor tapes, in *Proceedings of PAC09, Vancouver, BC, Canada* (IEEE, New York, 2009).
[8] T. A. Prikhna, Properties of MgB_2 bulk, arXiv:0912.4906.
[9] M. Majoros, M. Sumption, M. Susner, S. Bhartiya, S. D. Bohnenstiehl, E. Collings, M. Tomsic, M. Rindfleisch, J. Phillips, D. Lyons *et al.*, A model superconducting helical undulator wound using a wind and react MgB_2 multifilamentary wire, IEEE Trans. Appl. Supercond. **19**, 1376 (2009).
[10] I. Kesgin, M. Kasa, Y. Ivanyushenkov, and U. Welp, High-temperature superconducting undulator magnets, Supercond. Sci. Technol. **30**, 04LT01 (2017).

[11] R. Kinjo, T. Kii, H. Zen, K. Higashimura, K. Masuda, K. Nagasaki, and H. Ohgaki, A bulk high-Tc superconductor staggered array undulator, in *Proceedings of FEL08, Gyeongju, Korea* (JaCOW, Geneva, 2008), https://accelconf.web.cern.ch/FEL2008/papers/thaau03.pdf.

[12] R. Kinjo, T. Kii, M. A. Bakr, K. Higashimura, K. Yoshida, S. Ueda, K. Masuda, K. Nagasaki, H. Ohgaki, T. Sonobe, and H. Zen, Numerical evaluation of bulk HTSC staggered array undulator by bean model, in *Proceedings of FEL09, Liverpool, UK* (JaCOW, Geneva, 2009), https://accelconf.web.cern.ch/FEL2009/papers/thob03.pdf.

[13] T. Kii, R. Kinjo, M. A. Bakr, T. Sonobe, K. Higashimura, K. Masuda, H. Ohgaki, K. Yoshida, and H. Zen, Proposal of a bulk HTSC staggered array undulator *AIP Conf. Proc. No.* 1234, 539 (2010).

[14] C. P. BEAN, Magnetization of high-field superconductors, Rev. Mod. Phys. **36**, 31 (1964).

[15] R. Kinjo, M. Shibata, T. Kii, H. Zen, K. Masuda, K. Nagasaki, and H. Ohgaki, Demonstration of a high-field short-period undulator using bulk high-temperature superconductor, Appl. Phys. Express **6**, 042701 (2013).

[16] R. Kinjo, K. Mishima, Y.-W. Choi, M. Omer, K. Yoshida, H. Negm, K. Torgasin, M. Shibata, K. Shimahashi, H. Imon, K. Okumura, M. Inukai, H. Zen, T. Kii, K. Masuda, K. Nagasaki, and H. Ohgaki, Magnetic property of a staggered-array undulator using a bulk high-temperature superconductor, Phys. Rev. ST Accel. Beams **17**, 022401 (2014).

[17] Trapped fields, in *High Temperature Superconductor Bulk Materials* (John Wiley & Sons, Ltd, 2006), Chap. 5, pp. 105–127, https://onlinelibrary.wiley.com/doi/pdf/10.1002/3527608044.ch5.

[18] P. Grant, M. Denhoff, W. Xing, P. Brown, S. Govorkov, J. Irwin, B. Heinrich, H. Zhou, A. Fife, and A. Cragg, Determination of current and flux distribution in squares of thin-film high-temperature superconductors, Physica C (Amsterdam) **229**, 289 (1994).

[19] W. Xing, B. Heinrich, H. Zhou, A. A. Fife, and A. R. Cragg, Magnetic flux mapping, magnetization, and current distributions of $YBa_2Cu_3O_7$ thin films by scanning hall probe measurements, J. Appl. Phys. **76**, 4244 (1994).

[20] M. Carrera, J. Amorós, X. Obradors, and J. Fontcuberta, A new method of computation of current distribution maps in bulk high-temperature superconductors: Analysis and validation, Supercond. Sci. Technol. **16**, 1187 (2003).

[21] R. J. Wijngaarden, H. J. W. Spoelder, R. Surdeanu, and R. Griessen, Determination of two-dimensional current patterns in flat superconductors from magneto-optical measurements: An efficient inversion scheme, Phys. Rev. B **54**, 6742 (1996).

[22] E. H. Brandt, Determination of currents in flat superconductors, Phys. Rev. B **46**, 8628 (1992).

[23] R. J. Wijngaarden, K. Heeck, H. Spoelder, R. Surdeanu, and R. Griessen, Fast determination of 2D current patterns in flat conductors from measurement of their magnetic field, Physica C (Amsterdam) **295**, 177 (1998).

[24] N. Takeda, M. Uesaka, and K. Miya, Influence of an applied magnetic field on shielding current paths in a high T_c superconductor, Cryogenics **35**, 893 (1995).

[25] D. K. Namburi, Y. Shi, and D. A. Cardwell, The processing and properties of bulk (RE)BCO high temperature superconductors: current status and future perspectives, Supercond. Sci. Technol. **34**, 053002 (2021).

[26] M. Calvi, M. D. Ainslie, A. Dennis, J. H. Durrell, S. Hellmann, C. Kittel, D. A. Moseley, T. Schmidt, Y. Shi, and K. Zhang, A GdBCO bulk staggered array undulator, Supercond. Sci. Technol. **33**, 014004 (2020).

[27] J. Rhyner, Magnetic properties and AC-losses of superconductors with power law current-voltage characteristics, Physica C (Amsterdam) **212**, 292 (1993).

[28] COMSOL Inc., COMSOL, http://www.comsol.com/products/multiphysics/ (2020).

[29] B. Shen, F. Grilli, and T. Coombs, Overview of *H*-formulation: A versatile tool for modeling electromagnetics in high-temperature superconductor applications, IEEE Access **8**, 100403 (2020).

[30] B. Shen, F. Grilli, and T. Coombs, Review of the AC loss computation for HTS using *H* formulation, Supercond. Sci. Technol. **33**, 033002 (2020).

[31] M. D. Ainslie and H. Fujishiro, Modelling of bulk superconductor magnetization, Supercond. Sci. Technol. **28**, 053002 (2015).

[32] S. Hellmann, M. Calvi, T. Schmidt, and K. Zhang, Numerical design optimization of short-period hts staggered array undulators, IEEE Trans. Appl. Supercond. **30**, 1 (2020).

[33] K. Zhang, M. Ainslie, M. Calvi, S. Hellmann, R. Kinjo, and T. Schmidt, Fast and efficient critical state modelling of field-cooled bulk high-temperature superconductors using a backward computation method, Supercond. Sci. Technol. **33**, 114007 (2020).

[34] Apache Common Math, https://commons.apache.org/proper/commons-math/ (2020).

[35] A. Conn, K. Scheinberg, and L. Vicente, Introduction to derivative-free optimization, MPS-SIAM series on optimization, *SIAM* (2009).

[36] M. J. Powell, The bobyqa algorithm for bound constraint optimization without derivatives, University of Cambridge, England Report No. DAMTP 2009/NA06, 2009.

[37] K. Zhang, M. Ainslie, M. Calvi, R. Kinjo, and T. Schmidt, Fully-staggered-array bulk Re-Ba-Cu-O short-period undulator: large-scale 3D electromagnetic modelling and design optimization using *A*-*V* and *H*-formulation methods, Supercond. Sci. Technol. **34**, 094002 (2021).

[38] https://chart.ch.